PHYSICAL REVIEW D

PARTICLES AND FIELDS

THIRD SERIES, VOLUME 40, NUMBER 10 15 NOVEMBER 1989

Results of a laboratory search for cosmic axions and other weakly coupled light particles

W. U. Wuensch,* S. De Panfilis-Wuensch,† Y. K. Semertzidis,
J. T. Rogers, and A. C. Melissinos
Department of Physics and Astronomy, University of Rochester, Rochester, New York 14627

H. J. Halama, B. E. Moskowitz, and A. G. Prodell
Brookhaven National Laboratory, Upton, New York 11973

W. B. Fowler and F. A. Nezrick
Fermi National Accelerator Laboratory, Batavia, Illinois 60510
(Received 8 June 1989)

A microwave cavity experiment designed to search for the signal from cosmic axions converting in an external magnetic field covered the mass range $(4.5-16.3)\times10^{-6}$ eV, corresponding to the frequency range from 1.09 to 3.93 GHz. Upper limits on the coupling and abundance of nonrelativistic galactic axions have been measured; these limits yield a coupling which is 1–2 orders of magnitude higher than that predicted by the Dine-Fischler-Srednicki model. Also presented are limits on axions with a continuum spectrum, limits on the presence of a wide axion line at the frequency of the 21-cm hydrogen emission line, and limits on the production of pseudoscalar particles by photons in the cavity interacting with the magnetic field.

I. LIGHT AXIONS AND DARK MATTER

There are a number of indications that there may be more mass present in the Universe than has been directly observed so far. As early as 1933, Zwicky pointed out that stars at large distances from the center of galaxies have higher than expected orbital velocities based on the estimated masses of the galaxies.[1] This discrepancy implies the existence of an unseen mass, which has subsequently been well established by the measurement of the rotation curves (orbital velocity as a function of radius) of numerous galaxies. Measurement of the motions of galaxies themselves within clusters also indicates the presence of mass in excess of what is observed. Finally, cosmological arguments indicate that the Universe should be flat: namely, $\Omega=\rho_0/\rho_c=1$; however, observed mass densities yield a value of Ω approximately equal to 0.01–0.1. Here ρ_0 is the present-day matter density and ρ_c is the critical density:

$$\rho_c=\frac{3H_0^2}{8\pi G}=5\times10^{-30}\ \text{g/cm}^3=10^4\ \text{eV/cm}^3\ , \qquad (1)$$

where a value of $H_0=50$ km/s Mpc is used for the Hubble constant.

Having accepted the presence of dark matter we consider of what it may consist. Primordial nucleosynthesis constrains the amount of the dark matter which could be baryonic. It is expected that the density of baryons at the time of nucleosynthesis determines the relative abundances of the elements D, ^{3}He, ^{4}He, and ^{7}Li which have been formed. This can be used to place a limit on the total density of baryons when the current relative abundances of the previously mentioned elements are considered. One finds

$$\Omega_b\leq0.2\ , \qquad (2)$$

where Ω_b is the fraction of the current closure density which is composed of baryons.[2] Of course it is still possible that any of the dark-matter problems on a smaller scale, such as galactic halos, could be solved with a form of dark baryonic matter without contradicting the limit in Eq. (2). There are observational constraints on this, but baryonic dark matter could be in the form of nonluminous "Jupiters." The pervasiveness of dark matter, however, suggests that its composition could be similar on all scales and is, most probably, nonbaryonic. In this case, dark matter could be composed of weakly interacting fundamental particles.

Among the known stable particles only the neutrino interacts weakly enough to be a dark-matter candidate, but

it must have a finite rest mass to provide closure (make $\Omega=1$). Dark-matter neutrinos would have had relativistic velocities at the time of structure formation and are classified as "hot" dark matter.[3] However, theories of the formation of structure in the Universe have difficulties when most of the mass is in the form of hot dark matter; density perturbations are smoothed out too quickly and observed structures do not form. Neutrinos therefore may not be a suitable dark-matter candidate. In addition, neutrinos cannot make up galactic halos because they are low-mass fermions: it is not possible to fill the gravitational potential of galaxies with enough neutrinos to produce the observed rotation curves. Recent theories of particle physics predict a rich selection of weakly interacting particles which could constitute dark matter, the prime candidate being the very weakly interacting axion.

The axion was introduced to explain the absence of *CP* (charge-conjugation-parity) violation in the strong interactions. The QCD (quantum chromodynamics) Lagrangian contains a term

$$L_\theta=\theta\tilde{G}^{\mu\nu}G_{\mu\nu}\ ,$$

which violates *CP*; here $G^{\mu\nu}$ is the gluon field tensor and θ is an angular coefficient with possible values between 0 and 2π. Measurements of the electric dipole moment of the neutron[4] place an experimental upper bound $\theta<10^{-9}$. To explain naturally why θ should be so small, Peccei and Quinn[5] introduced an approximate global symmetry into the QCD Lagrangian making θ a dynamical variable. Peccei-Quinn (PQ) symmetry is not observed in nature because it was spontaneously broken already at very high temperatures, causing θ to oscillatte around its minimum value, $\theta=0$. As pointed out independently by Weinberg and Wilczek,[6] a necessary consequence of the spontaneous breaking of the approximate PQ symmetry is the generation of a nearly massless pseudoscalar particle, dubbed the axion. The axion is a pseudo-Goldstone boson which would be massless if the PQ symmetry had been exact before spontaneous symmetry breaking had occurred. The axion mass is related to the symmetry-breaking scale F_a through

$$m_a=m_\pi\left[\frac{F_\pi}{F_a}\right]N\frac{\sqrt{z}}{1+z}\approx 2\times10^{-5}\ \text{eV}\left[\frac{10^{12}\ \text{GeV}}{F_a}\right]. \tag{3}$$

In Eq. (3), $F_\pi\approx93$ MeV is the pion decay constant, N is the number of quark families which we set as $N=3$, and $z=m_u/m_d\approx\frac{1}{2}$ is the mass ratio of the light quarks.

In general, axions couple to fermions with a strength $g_a\sim1/F_a$ but the details of the coupling are model dependent. It was originally believed that the PQ symmetry breaks at the weak-interaction scale, but experiments using charged-particle beams[7] have ruled out the mass range $m_a>6$ keV. Soon thereafter, Kim[8] and independently Dine, Fischler, and Srednicki[9] (DFS) pointed out that the PQ-symmetry-breaking scale could be much larger, making the axion extremely light and its coupling extremely weak. Such light axions were called "invisible" and they were found to have important astrophysical and cosmological manifestations. Axions couple to two photons through the triangle anomaly shown in Fig. 1(a), with effective strength

$$g_{a\gamma\gamma}=\frac{\alpha N}{2\pi F_a}\left[\bar{c}_{a\gamma\gamma}-\frac{2}{3}\frac{4+z}{1+z}\right], \tag{4}$$

where $\bar{c}_{a\gamma\gamma}$ is the ratio of the charge-to-color anomaly of Peccei-Quinn symmetry.[10] With $z=\frac{1}{2}$ and $\bar{c}_{a\gamma\gamma}=\frac{8}{3}$, as in the DFS and most hadronic models, we find

$$\begin{aligned}g_{a\gamma\gamma}&=m_a\left[\frac{e^2}{\hbar c}\right]\frac{(\hbar c)^{3/2}}{F_\pi m_\pi}\frac{1}{\pi\sqrt{2}}\\&=(1.1\times10^{-34}\ \text{MeV}^{1/2}\text{cm}^{3/2})\frac{m_a}{10^{-5}\ \text{eV}}\\&=(1.3\times10^{-15}\ \text{GeV}^{-1})\frac{m_a}{10^{-5}\ \text{eV}}\ .\end{aligned} \tag{5}$$

This yields a free axion lifetime

$$\begin{aligned}\tau(a\rightarrow\gamma\gamma)&=\tau(\pi^0\rightarrow\gamma\gamma)\left[\frac{m_\pi}{m_a}\right]^5N^4\frac{z^3}{1+z^4}\\&\sim10^{49}\ \text{s}\left[\frac{F_a}{10^{12}\ \text{GeV}}\right]^5,\end{aligned} \tag{6}$$

which is sufficiently long to allow for observation, in the present era, of primordially produced axions with mass less than 40 eV.

The existence of such light axions would have impor-

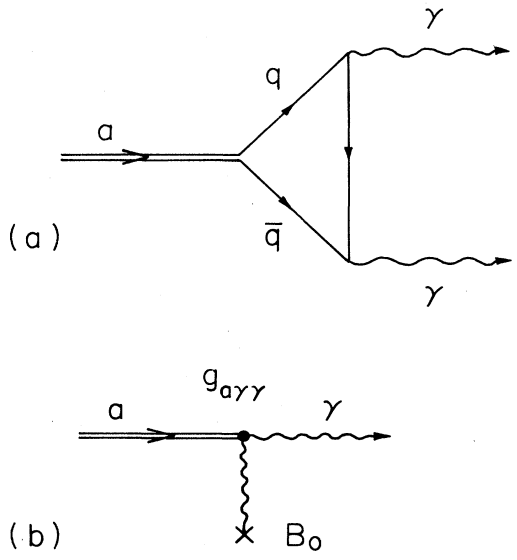

FIG. 1. (a) Two-photon coupling of axion through triangle anomaly. (b) Axion conversion via Primakoff effect.

tant consequences for stellar evolution. Because of their weak coupling, axions produced in bremsstrahlung processes in the hot interiors of stars would escape without interacting, cooling the stars too quickly. Similarly, the energy carried away from supernova 1987A by neutrinos can be used to place a limit on axion production in SN 1987A and thus a limit on axion mass and coupling.[11] The current limits on the mass of the axion are summarized in Fig. 2 and indicate that $m_a \leq 10^{-3}$ eV for DFS axions. The lower limit of $m_a \geq 10^{-6}$ eV derives from the requirement that the Universe not be overclosed.[12] Axions should have been produced in the early Universe as the temperature cooled below a temperature of order F_a and Peccei-Quinn symmetry was broken. The axion mass arises from instanton effects which produced the potential for θ and which commenced at a temperature of the order of the quark-hadron transition energy (~ 1 GeV); at this time coherent oscillations of the Bose axion field developed. The value of the mass which exactly closes the Universe with axions has uncertainties in the Hubble constant, the quark-hadron transition energy, and the dynamics of the transition, but may be summarized by[13]

$$2.5\times10^{-6} \leq m_a \leq 6.5\times10^{-5} \text{ eV} , \tag{7}$$

with $m_a \sim 10^{-5}$ eV being the most likely value.

As the Universe continued to expand, the axions should have condensed into galactic halos. Since their interactions are so weak, their velocity is determined solely by gravitational equilibrium, and is given by the galactic virial velocity. Near Earth this velocity is observed[14] to be $v \sim 10^{-3}c$. Thus the axions will have a narrow, nonrelativistic energy distribution characterized by

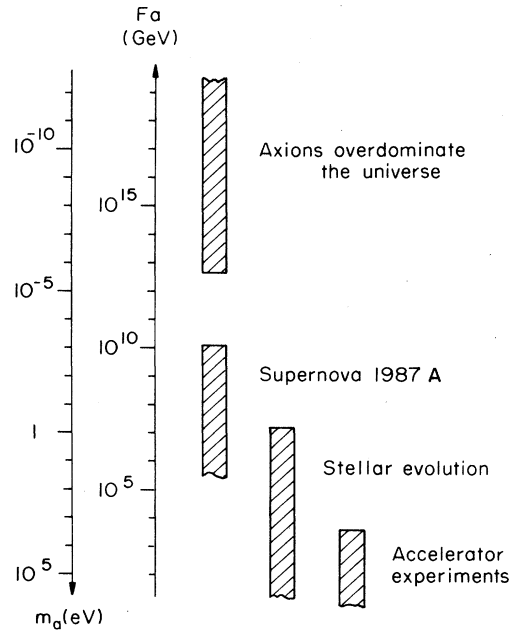

FIG. 2. Summary of the limits on the mass of the axion. The limit from supernova 1987A is for the DFS model only.

$$Q_a \equiv \frac{E_a}{\Delta E_a} = \frac{m_a c^2}{m_a v^2/2} \approx 2\times10^6 . \tag{8}$$

A previous result[15] of $Q_a = 9\times10^6$ is in error[16] due to a missing factor of $(2\pi)^{-1}$. The expected density of axions near Earth in an isothermal spherical halo model has been calculated by Turner[13] to be

$$\langle \rho_a \rangle = 5\times10^{-25} \text{ g/cm}^3 = 300 \text{ MeV/cm}^3 . \tag{9}$$

II. CAVITY DETECTORS

Direct detection of axions decaying into two photons is extremely difficult, as seen by the lifetime in Eq. (6). However, following a proposal of Sikivie,[17] it is possible to supply a virtual photon from a strong externally applied magnetic field and detect the decay of the axion into the second photon via a Primakoff-type effect.[18] The Feynman diagram for this process is shown in Fig. 1(b). By conservation of energy, the frequency of the real photon produced is given by

$$f = \frac{E_a}{h} \approx \frac{m_a}{h} , \tag{10}$$

where h is Planck's constant; note that for $m_a = 1\times10^{-5}$ eV, we have $f = 2.4$ GHz, which is in the microwave S band. To most effectively trap this photon for detection and enhance the $a \rightarrow \gamma$ conversion rate, a resonant microwave cavity may be used.

The following derivation of the expected signal power in the cavity follows Ref. 15. The interaction Lagrangian between the electromagnetic and axion fields is given (in Gaussian units) by

$$\mathcal{L}_{\text{int}} = -\frac{g_{a\gamma\gamma}}{4\pi} \mathbf{E}_\gamma \cdot \mathbf{B}_{\text{ext}} \phi_a , \tag{11}$$

where $\mathbf{E}_\gamma$ is the electric field of the outgoing photon, $\mathbf{B}_{\text{ext}}$ is the external magnetic field, and ϕ_a is the axion field which can be expressed in terms of the local axion density through

$$\langle \rho_a \rangle = m_a^2 \int_{-\infty}^{\infty} |\phi_a(t)|^2 dt . \tag{12}$$

The equation of motion in the presence of an external magnetic field B_{ext} is

$$\nabla^2 E - \frac{1}{c^2}\frac{\partial^2 E}{\partial t^2} = \frac{g_{a\gamma\gamma}}{c^2} B_{\text{ext}} \frac{\partial^2 \phi_a(t)}{\partial t^2} . \tag{13}$$

We solve Eq. (13) inside a resonant cavity by standard methods:

$$\nabla^2 E(x,\omega) + \frac{\omega^2}{c^2} E(x,\omega) = -g_{a\gamma\gamma} B_{\text{ext}} \frac{\omega^2}{c^2} \phi_a(\omega) , \tag{14}$$

$$\phi_a(\omega) = \int_{-\infty}^{\infty} \phi_a(t) e^{i\omega t} dt . \tag{15}$$

The boundary conditions of the cavity and energy dissipation caused by finite Q result in a steady-state energy U_j in the cavity for the jth mode:

$$U_j = g_{a\gamma\gamma}^2 G_j^2 V B_0^2 \int \frac{|f_a(\omega)|^2 \omega^4}{(\omega-\omega_j)^2 + \omega^4/Q^2} \frac{d\omega}{4\pi} , \tag{16}$$

where B_0^2 is the average of the square of the magnetic field inside the cavity:

$$B_0^2=\frac{1}{V}\int |B_{\rm ext}(x)|^2 d^3x \ , \tag{17}$$

V is the cavity volume, and G_j^2 is defined by the integral

$$G_j^2=\frac{1}{B_0^2 V}\frac{\left[\int \mathbf{B}_{\rm ext}\cdot\mathbf{E}_j d^3x\right]^2}{\int \mathbf{E}_j\cdot\mathbf{E}_j d^3x} \ , \tag{18}$$

for the jth mode of the cavity. The quantity G_j^2 is a form factor which measures the alignment of the electric field in the cavity with the external magnetic field.

The total power produced in the mode j due to axion conversion is given (in mks units) by

$$P_0=\left[\frac{g_{a\gamma\gamma}}{m_a}\right]^2 \langle\rho_a\rangle \omega_a \min\{Q_L,Q_a\}\epsilon_0(cB_0)^2 V G_j^2 \ , \tag{19}$$

where $\omega_a\equiv m_a/\hbar\equiv 2\pi f_a$, and Q_L is the *loaded* cavity quality factor.

The actual power P_r detected by a receiver depends on its coupling strength to the cavity mode.[19] For simplicity and convenience we consider critical coupling, for which

$$P_r=\tfrac{1}{2}P_0 \ . \tag{20}$$

With realistic parameters, we expect the signal

$$P_r=(2.2\times10^{-24}\ \text{W})\left[\frac{\langle\rho_a\rangle}{5\times10^{-25}\ \text{g/cm}^3}\right]\left[\frac{f_a}{1\ \text{GHz}}\right] \times\left[\frac{B_0}{6\ \text{T}}\right]^2\left[\frac{V}{10^4\ \text{cm}^3}\right]\left[\frac{Q_L}{10^5}\right]\left[\frac{G_j^2}{0.7}\right] \ . \tag{21}$$

The choice of cavity mode is an important one since most modes have symmetries which imply $G_j^2=0$. Also of importance is the ability to *tune* the resonant frequency of the cavity over a wide range (while maintaining high Q) since the width of the axion line is very narrow, and its frequency (mass) is uncertain to 3 orders of magnitude, as in Fig. 2. We have used a right-cylindrical cavity operating in a TM_{0m0} mode and tuned it by inserting along its symmetry axis a rod of a high dielectric material. The form factor for such a mode in the untuned (no rod) case is given by

$$(G^2)_{TM_{0m0}}=\frac{4}{(x_{0m})^2} \ , \tag{22}$$

where x_{0m} is the mth zero of the Bessel function J_0. The untuned TM_{010} mode is shown in Fig. 3 and has $G^2=0.7$. As the tuning rod is inserted, the electric field lines of the mode are distorted; numerical solutions to Maxwell's equations done by computer show that G^2 for our geometry does not change by more than a factor of 2 during the tuning process for the TM_{010} mode, and actually improves for the TM_{020} mode.[16]

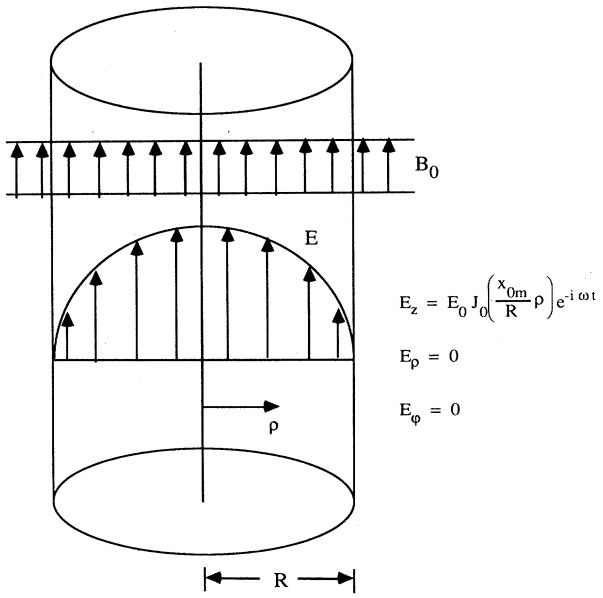

FIG. 3. TM_{010} mode of a right-cylindrical cavity with an external magnetic field aligned along the cavity axis.

III. DESCRIPTION OF THE APPARATUS

The frequency range from 1.090 to 3.933 GHz (which corresponds to $4.510\le m_a\le 16.27\times10^{-6}$ eV) was covered using seven microwave cavities, as summarized in Table I. (A gap from 2.460 to 2.732 GHz was not covered by the data presented here.) The first results of

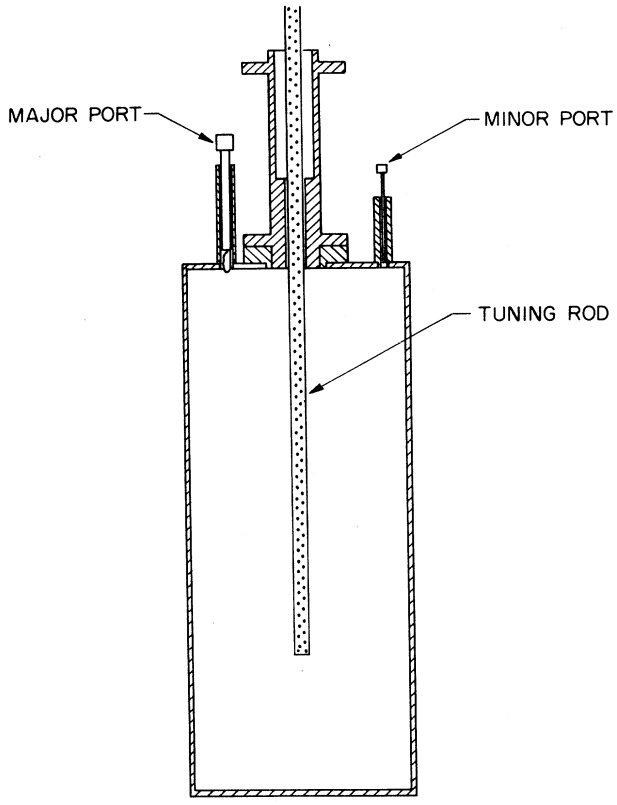

FIG. 4. Cross section of microwave cavity.

TABLE I. Experimental limits on cosmic axion abundance and coupling. Listed for each cavity-rod combination are the parameters used. All cavities were 40 cm in length. The values for the loaded quality factor Q_L, the form factor G^2, and the rms deviation of the noise, σ_{local}, are typical values for the frequency ranges given. Unless otherwise noted, the TM_{010} mode was used.

Cavity No.	Cavity diameter (cm)	Rod diameter (cm)	Δf (Hz)	B_0 (T)	f (GHz)	Percent coverage	Q_L	G^2	σ_{local} (W/Hz)	N_σ checked	95%-C.L. upper limits $(g_{a\gamma\gamma}/m_a)^2\rho_a$	$g_{a\gamma\gamma}$ $(\text{GeV}^{-1})^a$
1	18.415	1.486	200	5.8	1.090–1.218	98.8	1.0×10^5	0.50	2.0×10^{-24}	5	5.9×10^{-41}	2.4×10^{-14}
2	15.876	1.486	200	5.8	1.218–1.320	93.9	4.6×10^4	0.50	2.9×10^{-24}	5	2.1×10^{-40}	5.0×10^{-14}
2	15.876	1.486	200	5.8	1.320–1.415	99.4	2.1×10^4	0.50	1.8×10^{-24}	5	2.7×10^{-40}	6.1×10^{-14}
3	13.335	1.486	400	7.5	1.414–1.450	98.5	4.9×10^4	0.45	3.3×10^{-24}	4	3.3×10^{-40}	7.1×10^{-14}
3	13.335	1.486	400	7.5	1.450–1.512	97.0	5.0×10^4	0.40	2.4×10^{-24}	4	2.7×10^{-40}	6.6×10^{-14}
3	13.335	1.016	400	7.5	1.513–1.600	99.0	6.5×10^4	0.48	3.5×10^{-24}	4	2.4×10^{-40}	6.6×10^{-14}
3	13.335	1.016	400	7.5	1.600–1.687	99.5	6.5×10^4	0.48	3.2×10^{-24}	4	2.1×10^{-40}	6.5×10^{-14}
4	10.795	1.486	400	7.5	1.686–1.720	99.9	4.2×10^4	0.45	1.7×10^{-24}	4	2.6×10^{-40}	7.4×10^{-14}
4	10.795	1.486	400	7.5	1.720–1.764	92.0	4.2×10^4	0.40	2.1×10^{-24}	4	3.5×10^{-40}	8.8×10^{-14}
4	10.795	1.016	400	7.5	1.761–1.900	96.1	4.5×10^4	0.49	4.0×10^{-24}	4	4.7×10^{-40}	1.1×10^{-13}
4	10.795	1.016	400	7.5	1.900–2.087	97.0	4.5×10^4	0.54	5.0×10^{-24}	4	4.9×10^{-40}	1.2×10^{-13}
5	9.157	1.016	400	7.0	1.952–2.100	97.9	1.8×10^4	0.50	2.0×10^{-24}	4	7.1×10^{-40}	1.5×10^{-13}
5	9.157	1.016	400	7.0	2.100–2.250	96.3	1.2×10^4	0.50	2.1×10^{-24}	4	1.0×10^{-39}	1.9×10^{-13}
5	9.157	0.635	400	7.0	2.239–2.360	96.1	7.4×10^4	0.45	1.9×10^{-24}	4	1.9×10^{-40}	8.7×10^{-14}
5	9.157	0.635	400	7.0	2.360–2.460	87.6	8.7×10^4	0.65	2.7×10^{-24}	4	1.6×10^{-40}	8.2×10^{-14}
1[b]	18.415	1.588 teflon	200	5.8	2.732–2.801	96.8	6.0×10^4	0.14	5.0×10^{-24}	5	3.3×10^{-40}	1.4×10^{-13}
6	6.985	0.635	400	7.5	2.803–3.107	96.8	6.8×10^4	0.40	6.0×10^{-23}	4	8.5×10^{-39}	7.4×10^{-13}
7	5.715	0.635	400	7.5	3.106–3.200	90.0	6.9×10^4	0.50	9.0×10^{-24}	4	1.4×10^{-39}	3.2×10^{-13}
7	5.715	0.635	400	7.5	3.200–3.700	95.1	3.5×10^4	0.28	6.0×10^{-24}	4	2.9×10^{-39}	5.1×10^{-13}
7	5.715	0.635	400	7.5	3.700–3.933	93.7	6.4×10^4	0.50	1.2×10^{-23}	4	1.6×10^{-39}	4.2×10^{-13}

[a]In natural units, assuming the local galactic halo density for axions.
[b]The TM_{020} mode was used.

this search using cavity 1 have previously been reported.[20]

A cross section of a typical cavity is shown in Fig. 4. The cavities were all manufactured from 99.996% pure oxygen-free electronic grade copper;[21] individual pieces were electron-beam welded or clamped together. To further reduce surface losses, the inner cavity walls were mechanically honed and then electrochemically polished using a commercially available electropolish.[22] A typical value of the unloaded quality factor Q_0 at 4.4 K was 2×10^5; the effect of the magnetic field on Q_0 was small (see the discussion in Sec. VII below.) Three openings through the top plate of the cavity allowed access by the tuning rod, a "major" port for coupling the cavity to the receiver, and a "minor" port for the injection of calibration signals.

Each of the two coupling ports consisted of a 50-Ω coaxial probe with an induction pickup loop on the end. These lay inside closely fitting tubes projecting up from the top plate. The diameters of the tubes were chosen such that the waveguide cutoff frequencies were well above the cavity resonant frequency. The vertical position of the major coupling loop in its tube, and hence the strength of the coupling, could be adjusted via an outside micrometer. For impedance matching, critical coupling was used throughout all measurements. The minor port coupling parameter $\beta=(Q_0-Q_L)/Q_L$ was set at approximately 10^{-3}–10^{-4}.

Each cavity was tuned by an appropriate dielectric rod which could be moved up or down along the cavity axis. All but one of the tuning rods were made of single-crystal sapphire,[23] which has a permittivity $\epsilon\approx10$; the exception was a Teflon rod ($\epsilon\approx2.1$) used in the tuning of the TM_{020} mode of cavity 1. (See Table I.) The typical length of a rod was 55 cm; the rods entered the cavities through the rod housing tube which also acted as a circular waveguide below cutoff. A Teflon bearing centered each rod in the housing and allowed smooth longitudinal movement. During data taking, the rod was driven by a 5-turn/cm precision ball screw rotated by a dc motor which was stepped-down 2400:1 by two reducers. A typical tuning curve of frequency versus rod position is shown in Fig. 5; the curve of unloaded cavity Q versus

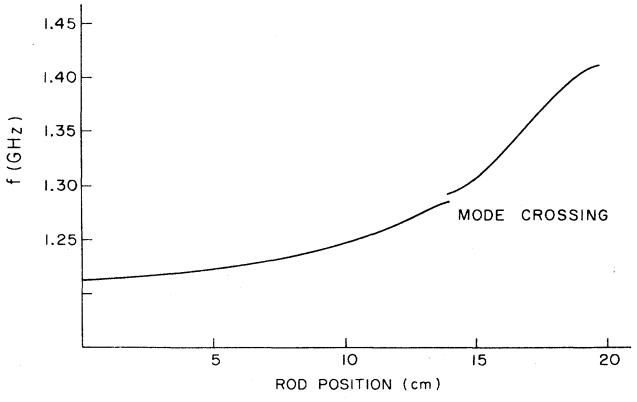

FIG. 5. Frequency vs rod position tuning curve.

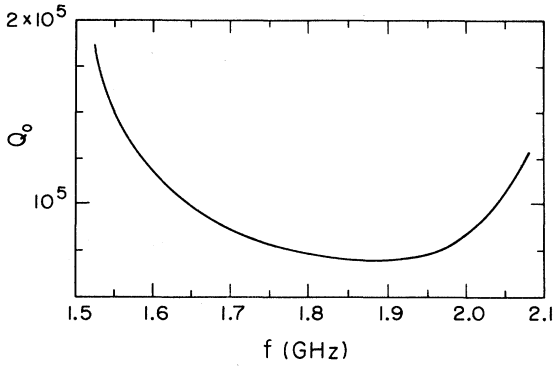

FIG. 6. Q vs frequency.

frequency is shown in Fig. 6.

Each cavity was placed inside the magnet bore as shown in Fig. 7. The magnet[24] had a 20-cm inner diameter and a 40-cm height, and was made of two coils of copper-stabilized superconducting NbTi. The magnet was operated with a current of 550 A which produced a peak field at the center of the bore of 6.7 T and a rms average field over the bore volume of 5.8 T. After performing measurements with cavities 1 and 2, an additional insert solenoid wound from kapton-wrapped NbTi monolith was added electrically in series. This reduced the inner bore to 15 cm while maintaining the same length. Measurements on cavities 3 through 7 were performed with a magnet current of 475 A which resulted in a peak field of 8.5 T and an rms average field of 7.5 T. The current was supplied from a Sorensen DCR20-1000A power supply and was monitored by a Holec zero-flux current transformer; a quench protection system was also

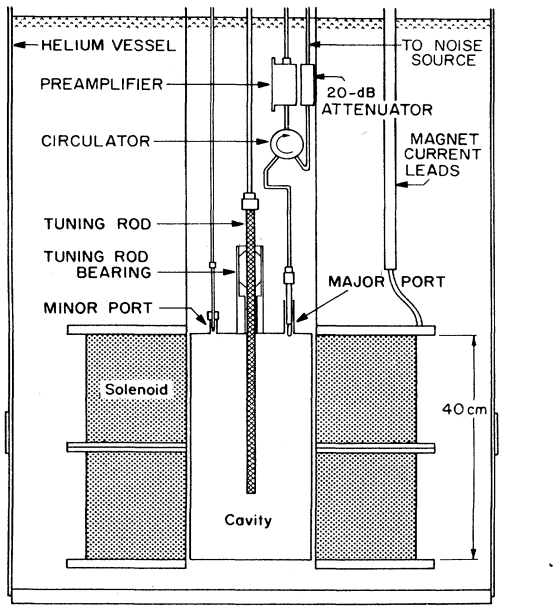

FIG. 7. The overall view of the detector: cavity+magnet.

included. The magnet leads were cooled by the boiloff helium gas from the experiment cryostat.

The output of the major port went directly to one arm of a cryogenic microwave circulator[25] which was used to impedance match the cavity to the microwave preamplifier. The arrangement is shown in Fig. 8. The second arm of the circulator was connected to a 20-dB attenuator which acted as a cold 50-Ω impedance. Upon reflection from the (critically coupled) major port, the Johnson noise from this impedance exactly complemented the thermal noise of the cavity to yield a flat spectrum. A diode noise source[26] with noise temperature of room temperature when off, and 11 315 K when on, was placed on the opposite side of the cold attenuator. Kept off during normal data taking, it was turned on only for gain calibration measurements of the detection electronics.

The third arm of the circulator went to a cryogenic three-stage GaAs field-effect-transistor (FET) preamplifier[27] whose design was based on amplifiers used by the National Radio Astronomical Observatory.[28] These amplifiers used packaged FET's and discrete components. Impedance matching was primarily accomplished through a network of coil inductors. Each FET was mounted on a copper finger, which provided a small source inductance to ground for additional matching. A stripline network at the input was used as a transformer. The amplifiers were tuned by deforming the inductors, moving grounding shims under the copper fingers, and moving a shorting termination on the stripline network. To tune the input impedance and gain, the amplifier was chilled in liquid nitrogen, as very little change in these parameters occurred between liquid-nitrogen and liquid-helium temperatures. The amplifier was then immersed in liquid helium to tune for minimum noise temperature. A description of the methods used to determine the amplifiers' cryogenic characteristics can be found in Ref. 27.

Seven different amplifiers were used in this search; for each combination of cavity and rod, an amplifier with optimal gain and noise characteristics in the appropriate bandwidth was chosen. The equivalent noise temperature of the amplifiers for the frequency range 1.0–2.7 GHz is shown in Fig. 9. A typical value of the preamplifier gain was 30 dB, with that figure varying within a cavity tuning bandwidth by ±5 dB.

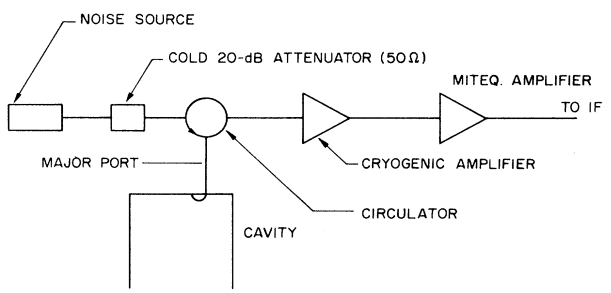

FIG. 8. Arrangement of the electronics connected through the circulator.

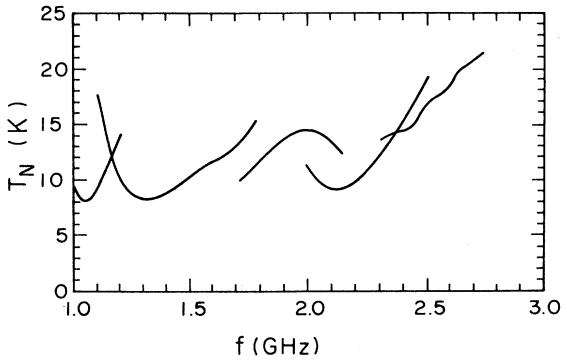

FIG. 9. Noise temperature coverage of preamps vs frequency for the range 1.0–2.7 GHz.

The remaining, room-temperature section of the detection electronics[16] can be seen in Fig. 10. In it, the microwave signal was mixed down to audio frequencies suitable for narrow-band detection. The first-stage local oscillator was a Hewlett-Packard (HP) model 8341A synthesizer whose microwave frequency was swept under computer control to track the resonant frequency of the cavity as it was tuned by the motion of the rod. The phase noise of this synthesizer was the dominant noise source in the system after the preamplifier; this necessitated sending the output of the cryogenic preamplifier through another stage of amplification[29] before mixing, and required that the local oscillator frequency be well separated from the cavity frequency. After mixing to an intermediate frequency near 10 MHz, the signal was further amplified by 60 dB, and mixed again with a 10-MHz local oscillator signal from a HP model 3325A synthesizer to a band with a 20-kHz low end. Both mixing stages were image-rejection type, composed of two quadrature hybrids and two mixers; the phase information retained by mixing in this way was used to reject the unwanted image frequency, which contained noise but no signal. The final quadrature hybrid, designed to operate in the 20-kHz range, was synthesized from operational-amplifier phase shifters.

Following the mixers was a 64-channel multiplexed filter/detector. Each channel contained a high-impedance unity-gain buffer, a variable-gain amplifier, a tunable active bandpass filter, a Schottky-barrier diode rectifier, and a low-pass integrating filter with time constant $\tau=RC=0.1$ sec. The 64 filters were tuned in ascending frequency from 20 kHz with a spacing equal to their bandwidth, and thus acted as a parallel spectrum analyzer. The channels were sequentially scanned by a HP 69752A FET scanner card and sampled by a HP 69751A analog-to-digital converter (ADC) which sent the data to a HP series 9000 microcomputer. The sampling time was chosen to match $\tau=0.1$ sec; hence the effective number of averages per ADC reading through the integrating filter is given by[30]

$$N_{\text{ave}}=\Delta f\tau\ , \tag{23}$$

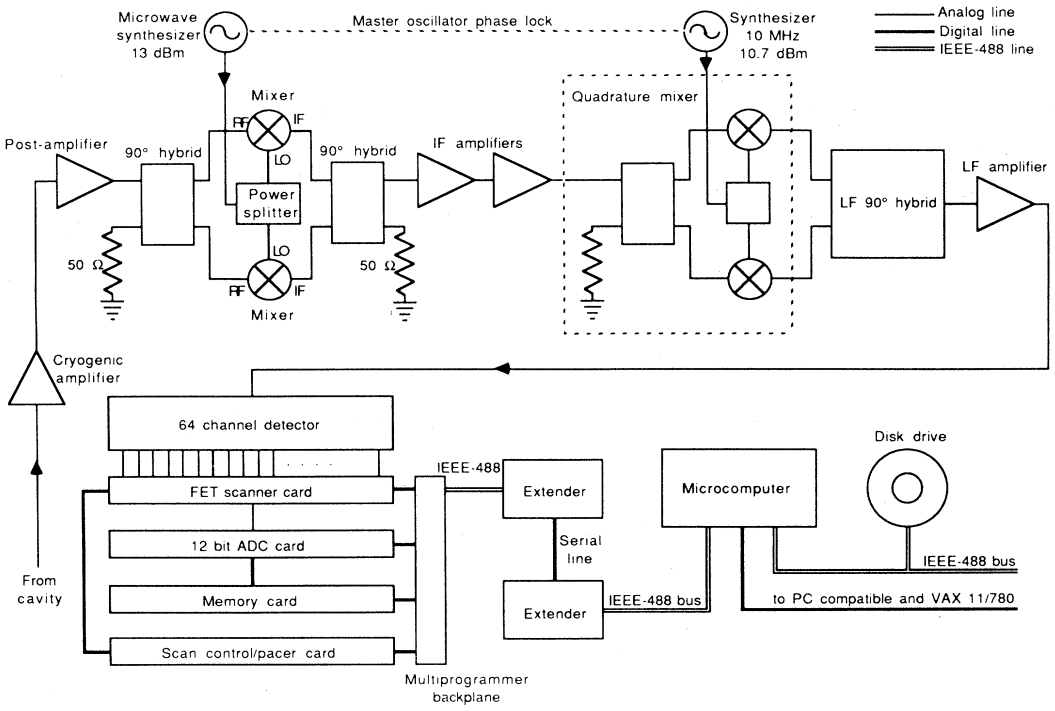

FIG. 10. Schematic of receiver electronics.

where Δf is the channel bandwidth. For cavities 1 and 2, $\Delta f = 200$ Hz was used; for all later cavities, $\Delta f = 400$ Hz.

The data-acquisition cycle[31] proceeded as follows: 32 768 ADC readings of the 64 channels were accumulated in a 65 536 word memory card, then transferred into an array in the HP microcomputer for reduction. During the data transfer and reduction, which involved summing the ADC readings into their proper microwave-frequency bins, the ADC sampling continued with no dead time. The data transfers occurred at 50-s intervals; staggered with them at 50-s intervals the microwave synthesizer output was momentarily routed through a set of coaxial relays to the cavity's minor port. The amplified output from the major port was similarly routed to a HP model 8757A network analyzer, which determined the resonant frequency from the peak of the transmission curve. The frequency and sweep rate of the microwave synthesizer were adjusted accordingly for the next 50-s interval. Thus the tuning rate was determined from the motion of the tuning rod, which was tracked in frequency by the synthesizer.

After 40 such 50-s cycles, the rod motion was halted and measurements were made through the coaxial relay network, noise source, and network analyzer of preamplifier gain, loaded cavity Q, and major port reflection coefficient. These data and the reduced ADC readings were then incorporated into a single file, sent to a Vax 11/780 via a dedicated IBM compatible PC for off-line analysis, and the cycle was started again. More details concerning the apparatus and data acquisition may be found in Refs. 16 and 31.

IV. NARROW-PEAK SEARCH RESULTS

In the following discussion, we define a *frequency channel* as one of the 64 parallel bands of the multiplexer-detector which sweep to track the cavity tuning, and a *frequency bin* as a fixed bin in absolute frequency. As the cavity resonance was swept through all the frequencies in its range, the on-line computer kept track of the power levels and number of ADC card readings for each reconstructed bin. Thus, the frequency power spectrum could be searched bin by bin for an axion conversion signal.

Figure 11 shows typical reconstructed spectra from two passes through a 400-kHz region taken with cavity 3. The height of each bin represents the power per unit frequency averaged over 400 Hz and the vertical error bars represent the statistical power fluctuation:

$$\sigma_n = \frac{P_n}{(N_{\mathrm{ADC}} \Delta f \tau)^{1/2}} , \tag{24}$$

where P_n is the measured power level in bin n, N_{ADC} is the number of ADC card readings in that bin, Δf is the multiplexer channel width, and τ is the multiplexer integration time constant (see the preceding section.) If the fluctuations in the power levels from the data are purely statistical, then the distribution of bin power levels, each normalized by σ_n, is a unit Gaussian. This is shown to be the case in Fig. 12, which is a histogram of the quantity $(P_n - P_{\mathrm{ave}})/\sigma_n$, where P_{ave} is the power level averaged over a neighborhood of ± 30 bins around bin n (Ref. 32).

To search the data for possible signals standing above

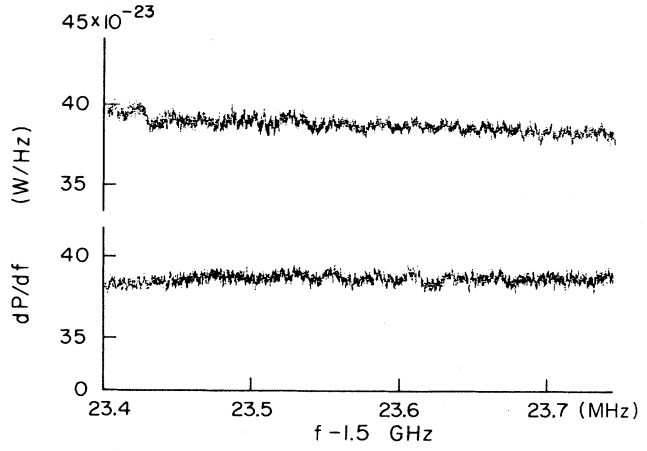

FIG. 11. Data from two passes of cavity 3 with 400-Hz frequency bins.

the background noise, we used a peak-searching algorithm whose figure of merit was

$$N_\sigma = \frac{P_n - P_{\text{ave}}}{\sigma_{\text{local}}} , \tag{25}$$

where σ_{local} is the observed rms deviation of the power level from the mean for a neighborhood of ± 30 bins around the bin in question.[33] All of the data were scanned by computer for bins above some threshold N_σ (either 4 and 5) and visually scanned and checked by eye on printouts. Coincidences between the two passes through the tuning range of the cavity-rod combination[34] were noted and a list of candidate peak frequencies produced. Each of these frequencies was studied in detail. By demanding the signal to be reproducible under normal data-taking conditions, absent without the magnetic field, and absent under off-resonance tuning conditions, all candidate peaks found were eliminated as possible axion conversion signals.

The calibration of the system was checked by placing test signals into the data. The signals were produced by a synthesizer coupled to the cavity via the minor port; readout occurred through the major port in the usual swept-frequency manner. Figure 13 shows the output data near an injected peak of total power 2×10^{-18} W and frequency 2.400 000 000 GHz. The agreement of the reconstructed frequency and total power under the peak with the respective known values from the synthesizer attests to the accuracy of the calibration procedure. Test signals were also used to confirm the validity of the peak-finding algorithm down to the 4σ level.

The absence of an axion conversion signal in our apparatus may be used to set a limit on the abundance and coupling of cosmic axions. In terms of the dimensionless quantity $(g_{a\gamma\gamma}/m_a)^2\rho_a$, it follows from Eqs. (19) and (20) that the 95%-confidence-level limit is given in mks units by

$$\left[\frac{g_{a\gamma\gamma}}{m_a}\right]^2 \rho_a < [(N_\sigma)_{\text{checked}} + 2]\frac{\mu_0}{\pi}\frac{1}{B_0^2 V}\frac{\sigma\Delta f}{CQ_L f_0}\frac{1}{G^2} , \tag{26}$$

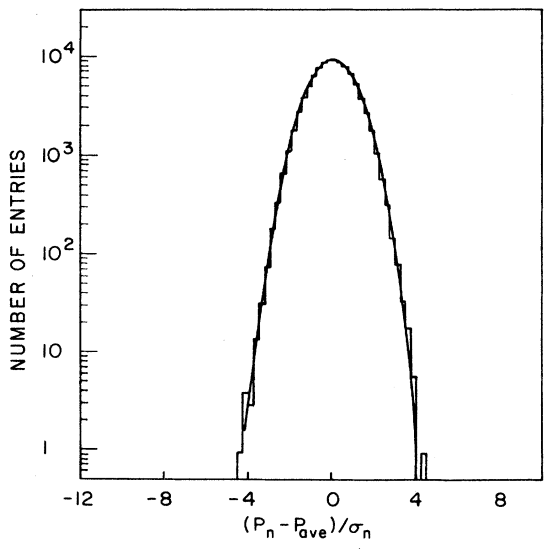

FIG. 12. Histogram of $(P_n - P_{\text{ave}})/\sigma_n$ from the first 100 000 bins of cavity 3. The superimposed curve is a Gaussian of unit width.

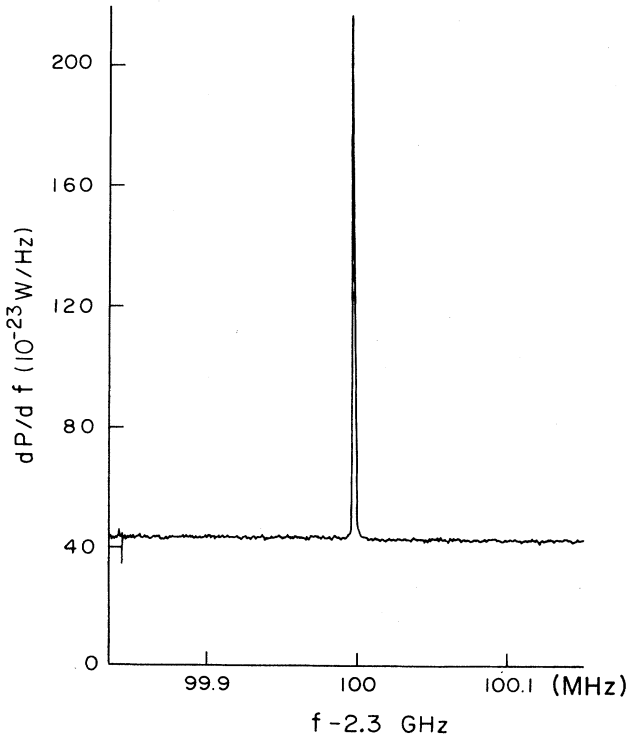

FIG. 13. An injected peak with a total power of 2×10^{-18} W at 2.400 000 000 GHz. The bin width is 400 Hz.

where $(N_\sigma)_{\text{checked}}$ is the threshold figure of merit used in peak checking, μ_0 is the permittivity in the cavity medium, B_0 is the magnetic field applied to the cavity, V is the cavity volume, σ is the value of σ_{local} in W/Hz as defined above, Δf is the multiplexer channel width, Q_L is the loaded cavity quality factor, f_0 is the central frequency of the bin, and G^2 is the form factor defined by Eq. (18). C is a correction due to the effect of the cavity line shape dropping off over the full bandwidth of the multiplexer as the sweep goes by; this is given by

$$C=\frac{2\Delta f_c}{\Delta f_m}\arctan\left[\frac{\Delta f_m}{2\Delta f_c}\right], \tag{27}$$

where $\Delta f_c=f_0/Q_L$ is the cavity full width at half maximum (FWHM), $\Delta f_m=N_m\Delta f$ is the full width of the multiplexer, and N_m=the number of multiplexer channels=64.

The limits on single-bin wide axion abundance and coupling are summarized in Table I. The values for Q_L, G^2, and σ are typical values for the frequency range given, with the form factor G^2 deriving from a numerical calculation with the program URMEL-T (Ref. 35). Note that the data covered 95%, in the typical case, and 88%, in the worst case, of the frequency range listed; the remaining "holes" were mostly regions where the cavity modes crossed, and the detection mode was unusable.[36] The upper limit on $(g_{a\gamma\gamma}/m_a)^2\rho_a$ from Eq. (26) is also listed in Table I; its value varies from 5.9×10^{-41} to 2.9×10^{-39} over the frequency range 1.090–3.933 GHz (Ref. 37). If one assumes the axions have sufficient density to provide all of the local galactic dark matter, as given by Eq. (9), then one finds the limit given for the coupling $g_{a\gamma\gamma}$ which is plotted in Fig. 14. The experimental limit is approximately 1–2 orders of magnitude greater than the prediction of the DFS model given in Eq. (5).

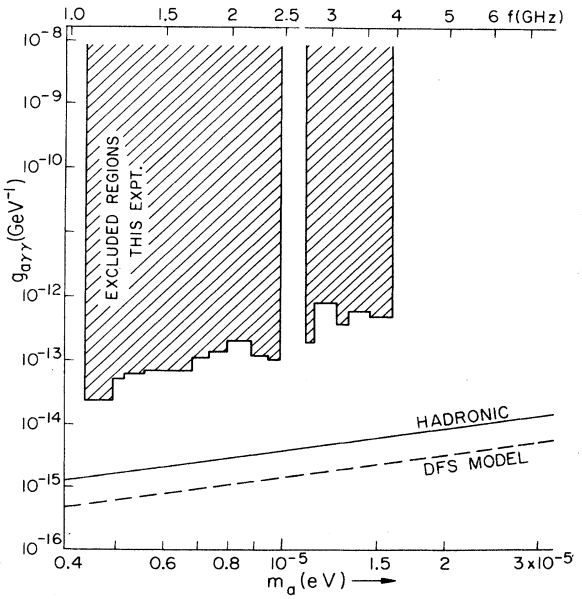

FIG. 14. Experimental limits on axion coupling versus frequency, assuming the density given by Eq. (9). The line labeled "DFS MODEL" shows the relationship of Eq. (5); the line "HADRONIC" shows Eqs. (3) and (4) with $\bar{c}_{a\gamma\gamma}=0$.

Since the actual width of the axion energy spectrum is not precisely known, we have also examined the possibility of a signal wider than a single multiplexer channel, Δf, existing in the data. The average power level was found for combined bins of width $2\Delta f$, $4\Delta f$, and $8\Delta f$, and the coincident peak-checking method applied as in the single-channel case. Again, no candidate peaks were found which survived the tests for being an axion conversion. The limits appropriate to the wider bins are given by Eq. (26) with $\Delta f\rightarrow2\Delta f$, $4\Delta f$, or $8\Delta f$; thus the upper limit on $g_{a\gamma\gamma}$ increases as (bin width)$^{1/2}$ up to the width of $8\Delta f$, which was 3.2 kHz for most cavity-rod combinations.

V. LIMITS ON AXIONS WITH A CONTINUUM SPECTRUM

It is natural to ask whether axions may also be distributed with a wide energy spectrum throughout the Universe. This would facilitate the search since it would not be necessary to tune the detector on the exact, but unknown, frequency corresponding to the axion mass. If this is the case, however, the spectral density is greatly reduced because the total number of axions is now spread over a much larger frequency band. Furthermore, since such axions would be relativistic, they could not condense into the galaxies, and as a result the expected galactic axion density in Eq. (9) would be reduced by a factor of $\sim10^5$. In spite of these arguments, assuming that light pseudoscalar particles ($m_a<10^{-5}$ eV) exist in the Galaxy, we present data that set a limit on the product of density times coupling.

In order to perform a measurement with the fixed cavity resonant frequency always centered in the detection electronics bandwidth, the apparatus described above was used with the following changes: First, the sapphire rod was kept stationary in cavity 3. The first local oscillator frequency was reset every 50 s to account for drifts. Typical drift between resettings was below 1 kHz while the long-term drift (which was corrected for) over the entire measurement did not exceed 20 kHz. Such shifts are completely irrelevant when searching for a signal with a broad frequency spectrum. Finally, the output from the receiver electronics was measured in a HP 5261 fast Fourier transform (FFT) spectrum analyzer instead of the 64-channel multiplexer. The FFT had 400 frequency channels covering the span of 0–100 kHz.

In principle, a difference in the microwave signal with the magnetic field on and with the magnetic field off would be an indication of a continuum signal. However, the magnetic field affects the circulator and amplifier,[38] and the overall signal level also depends on the liquid-helium level in the cryostat. Further, modulating the magnetic field at a rapid rate was impractical in our apparatus. An alternative technique was to compare the power level with the receiver tuned on the cavity resonance to that with the receiver tuned off resonance. In a

perfectly balanced system, these power levels should be flat and exactly equal in the absence of a signal in the cavity. However, because of the difference between the temperature of the circulator load (attenuator plus noise source) and that of the cavity, there is a residual 15% imbalance when tuned on resonance. To account for these effects we use the data off resonance to determine the effects of the magnetic field. We then use that calibration to correct the on-resonance data; this makes it possible to compare with high precision the data with the receiver tuned on the cavity resonance, both with and without the magnetic field.

The data from the continuum search are shown in Figs. 15 and 16 as follows: Fig. 15 refers to data with the full magnetic field of 7.5 T; Fig. 15(a) is on resonance and 15(b) is off resonance. The off-resonance data are shifted by 200 kHz from the cavity center. However the bandpass of the I.F. circuits is barely 100 kHz so that some distortions[39] can be expected at the two ends of the spectrum. Figures 16(a) and 16(b) give the same data but with zero magnetic field. They are similar to those with full field except for an overall reduction in power level by $\Delta T \approx 0.5$ K.

With the detector tuned on the cavity resonance the cavity shape is discerned as a dip of $\Delta T \approx 2$ K; the dip is absent in the off-resonance data where only an overall frequency dependence is present.[39] The absolute level of the power spectral density is referred to the input of the first amplifier (dominated by its internal noise) and was obtained by calibrating the entire detection chain. Data were acquired alternately between the on- and off-resonance conditions every 50 s and the two spectra (on and off) were acquired over a 10-h period.

To calibrate the data we divide the on-resonance data by the off-resonance data; the ratios are shown in Fig. 17 with the ratio for the full magnetic field shown in the solid line, and the ratio for zero magnetic field shown as the dotted line. These curves reflect the imbalance of the

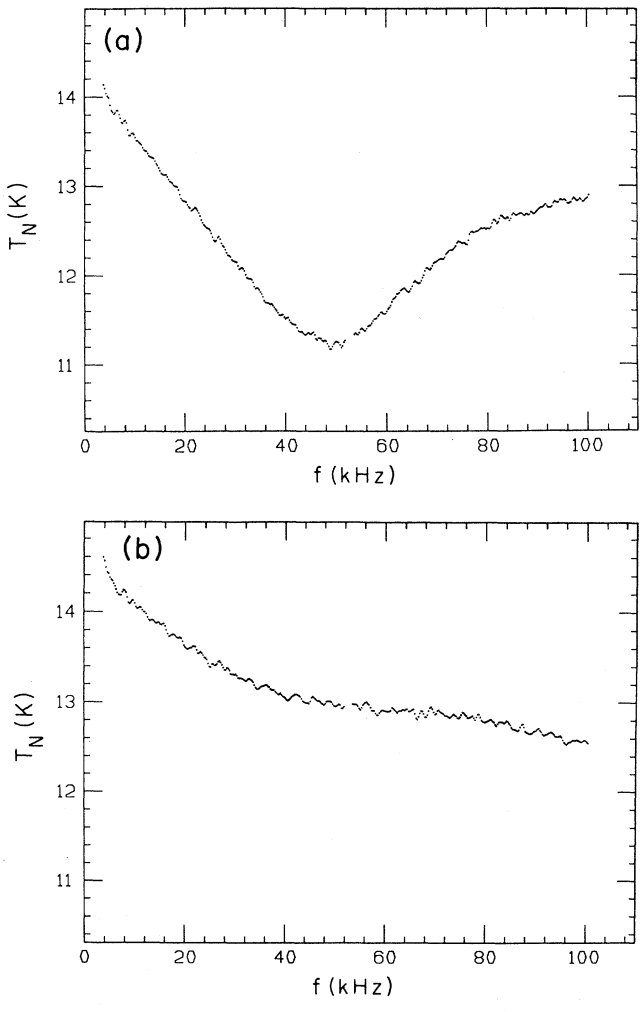

FIG. 15. Data at fixed frequency $f = 1.6700$ GHz with the magnetic field on: (a) on resonance, (b) off resonance.

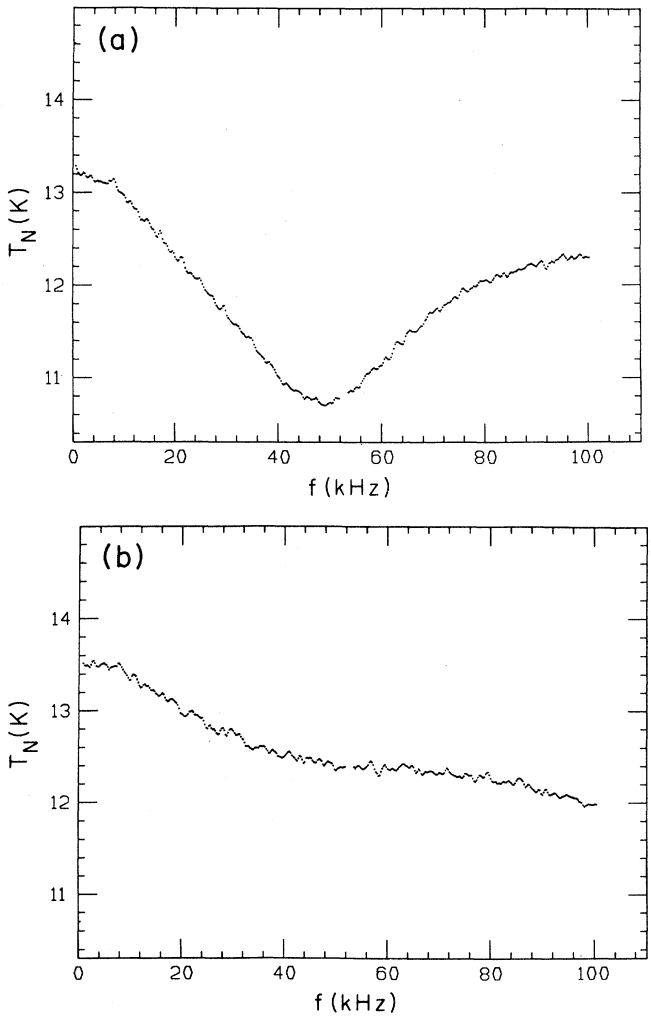

FIG. 16. Data at fixed frequency $f = 1.6700$ GHz without the magnetic field: (a) on resonance, (b) off resonance.

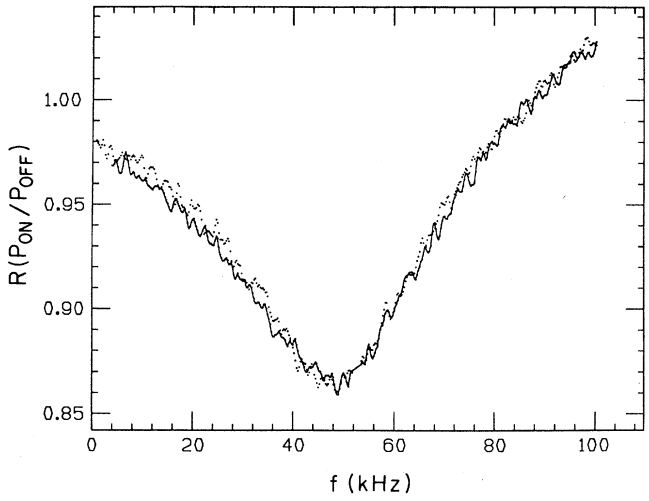

FIG. 17. Comparison of the normalized ratios of the data with magnetic field on (solid line) and without magnetic field (dotted line).

system and have a width $\Delta f = 35$ kHz. They *do not* reveal an increase in the power when the magnetic field is on. Indeed, Fig. 17 makes it clear that any systematic relative change in noise temperature, $\Delta T/T$, is less than 1%. A simple subtraction over the entire spectrum averaged over all 400 channels gives

$$\Delta T/T = -0.0031 \pm 0.0047 , \tag{28}$$

where $\Delta T = T(B_0 = 7.5T) - T(B_0 = 0)$, and the error quoted is the rms deviation from the mean.

The spectra are the average of 400 FFT cycles, every cycle corresponding to the average of 500 measurements. Thus the fluctuations in each channel should be $\delta P/P \approx 2.2 \times 10^{-3}$. The results of Eq. (28) are based on averaging 400 channels of the difference of two spectra and therefore its statistical uncertainty is

$$\delta\left[\frac{\Delta T}{T}\right] = \frac{1}{\sqrt{400}}\sqrt{2}\frac{\delta P}{P} \approx 1.6 \times 10^{-4} .$$

The larger value obtained experimentally indicates the presence of nonstatistical fluctuations; thus longer integration time would not improve on the limit of Eq. (28).

We adopt twice the error of $\delta(\Delta T/T)$ as found in Eq. (28) as the 95% confidence limit of the spectral density contributed by a continuum axion signal,[40] and use $T \approx 12$ K to find

$$\frac{dP_a}{df} < 1.7 \times 10^{-24} \text{ W/Hz} \tag{29}$$

at a frequency $f = 1.670$ GHz. To convert this power level to limits on axion density or coupling we use the conversion formula

$$\frac{dP_a}{df} = (3.4 \times 10^{-24} \text{ W/Hz}) \left[\frac{f}{1 \text{ GHz}}\right] \left[\frac{V}{10^4 \text{ cm}^3}\right] \times \left[\frac{Q_L}{10^5}\right] \left[\frac{G^2}{0.7}\right] \left[\frac{B_0}{8.5 \text{ T}}\right]^2 \times \left[\frac{\langle d\rho/df \rangle_a}{300 \text{ MeV/cm}^3\text{Hz}}\right] , \tag{30}$$

where $\langle d\rho/df \rangle_a$ is the spectral energy density due to the axions; furthermore we assumed that the axion coupling is related to its mass through Eq. (5) and that $m_a \sim 2\pi\hbar f$. For the parameters of our apparatus we find that the limit of Eq. (29) implies

$$\left\langle \frac{d\rho}{df} \right\rangle_a \Bigg|_{f=1.67 \text{ GHz}} \leq 400 \text{ MeV/cm}^3\text{Hz} . \tag{31}$$

The spectral distribution is of course unknown and therefore it is impossible to integrate Eq. (31) in order to obtain the total energy density. If we make the simplest assumption, $\Delta f \approx f$, we are led to $\rho_a \leq 7 \times 10^{17}$ eV/cm^3. For comparison the present era photon density in the galaxy is $\rho_\gamma \approx 1$ eV/cm^3 whereas the closure density of the Universe is $\rho_c = 3.5 \times 10^3$ eV/cm^3.

If we relax the theoretical prediction for the axion coupling in terms of its mass we write, instead of Eq. (30),

$$\frac{dP_a}{df} = (1.3 \times 10^{-24} \text{ W/Hz}) \left[\frac{g_{a\gamma\gamma}}{10^{-15} \text{ GeV}^{-1}}\right]^2 \times \left[\frac{\langle d\rho/df \rangle_a}{300 \text{ MeV/cm}^3\text{Hz}}\right] \tag{32}$$

evaluated for the parameters of our apparatus and at

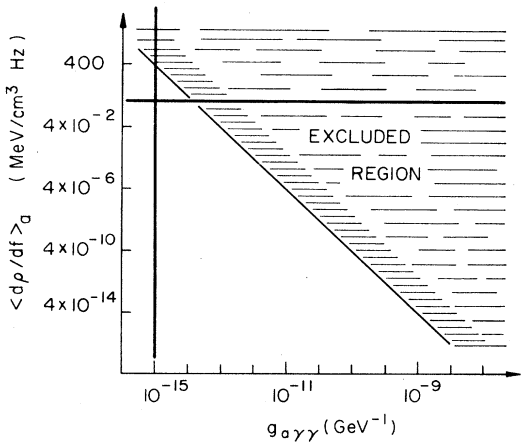

FIG. 18. Plot of the excluded region of energy spectral density $\langle d\rho/df \rangle_a$ and coupling $g_{a\gamma\gamma}$. The bold horizontal line indicates the predicted spectral density for quasimonochromatic cold axions that have condensed into the galaxies. The bold vertical line indicates the predicted DFS coupling for axions with a mass equal to the detector frequency. Note that the intersection of the two lines lies in the allowed region.

$f=1.670$ GHz. Note that $g_{a\gamma\gamma}$ in Eq. (32) is expressed in natural units; if multiplied by $(\hbar c)^{3/2}$, it will acquire the full dimensions. Thus our observational limit of Eq. (29) constrains the product

$$g_{a\gamma\gamma}^2\langle d\rho/df\rangle_a < 4\times10^{-28}\ \text{GeV}^{-2}\text{MeV cm}^{-3}\text{Hz}^{-1}\ .$$

This result is plotted in Fig. 18 showing the excluded region. As a reference the spectral density of the 3-K cosmic background radiation at this frequency is $\sim10^{-23}$ MeV/cm^{3}Hz; the spectral density of axions condensed into the galaxies, assuming a narrow line of width $\Delta f=300$ Hz ($d\rho/df=1$ MeV/cm^{3}Hz), is indicated by the bold horizontal line. The bold vertical line indicates the expected DFS coupling at this frequency if the axions are cold. The limit on $g_{a\gamma\gamma}$ from solar evolution is at $g_{a\gamma\gamma}<10^{-9}$ GeV^{-1} whereas from SN 1987A Turner[11] obtains $g_{a\gamma\gamma}\leq10^{-11}$ GeV^{-1}.

VI. LIMITS ON THE PRESENCE OF A WIDE AXION LINE AT 1.4204 GHz

Another possibility is that light axions could be produced by the conversion of electromagnetic radiation in the intergalactic magnetic field. In this case the energy of the produced axion would equal the energy of the original photon, provided that the mass of the axion is less than or equal to the original photon energy. More specifically, a conversion signal in the cavity detector could be expected at the frequency of the 21-cm hydrogen emission line: namely, 1.4204 GHz. However, using the estimated value of $g_{a\gamma\gamma}$, the resulting axion flux is well below our detection capability. The advantage of such a search is that the frequency and spectral width of the line (typically $\Delta f\sim1$ MHz) are known for several astronomical sources. We report here on the results from a search for a broad axion line[41] in the vicinity of $f=1.4204$ GHz.

The data were taken by sweeping the frequency at a rate of 400 Hz/s and were recorded with a resolution of 400 Hz. However, since we are searching for a signal of width $\Delta f\sim1$ MHz, the data have been combined in bins of 10 kHz width. Figures 19(a) and 19(b) show two sweeps with the full magnetic field whereas Fig. 19(c) shows the same sweep with no magnetic field. The small differences (less than 10%) of the detected power for the three sweeps correlate well with the helium level and are of no significance by themselves.[42] The local fluctuations in the data have a rms value $\sigma\approx0.2$ K which is about ten times larger than expected statistically, since each point represents approximately 6×10^5 averages.

The galactic hydrogen emission line is expected at $f=1.4205$ GHz with only a small Doppler shift (≤0.5 MHz) and FWHM~1 MHz. No such structure is apparent in Figs. 19(a) and 19(b). While there are qualitative differences between the spectra with the magnetic field on [Figs. 19(a) and 19(b)], and without the field [Fig. 19(c)], these cannot be attributed to a signal. They are two low in amplitude and too broad in width; furthermore such slow modulation is typical of our data records at all frequencies.

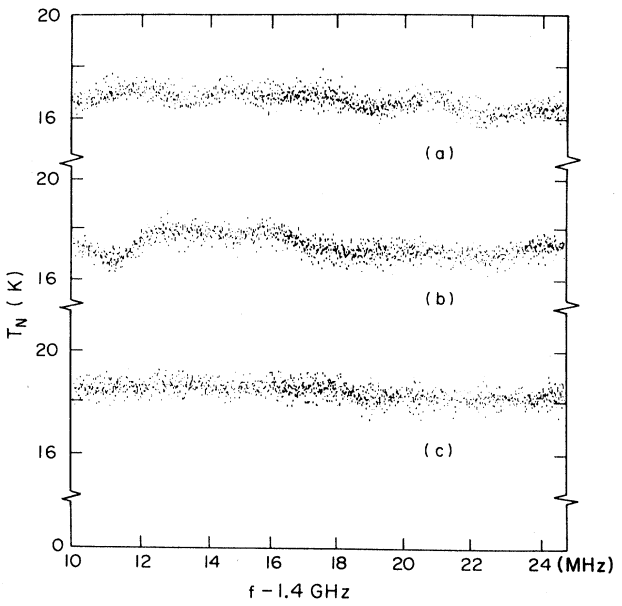

FIG. 19. Data obtained by sweeping the detector frequency in the region of the 21-cm hydrogen emission line ($f=1.404$ GHz). (a) and (b) are two different sweeps with the magnetic field on; (c) is a sweep without a magnetic field.

From the data we can conservatively exclude a signal of peak amplitude $\Delta T_s>0.5$ K. If we assume a width $\Delta f=0.5$ MHz we have $P_a<4\times10^{-18}$ W. Thus from Eq. (30) the axion energy density is $\rho_a\leq10^9$ MeV/cm^3, corresponding to a number density of $n_a\leq10^{20}$ axions/cm^3. For comparison the galactic photon flux at this frequency is $F_\gamma\approx10^6$–10^7 cm^{-2}s^{-1} leading to a photon density of order $n_\gamma\sim10^{-4}$ cm^{-3}. It is therefore evident that even if the axion density equals the galactic photon density, the coupling would have to be of order $g_{a\gamma\gamma}\sim10^{-3}$ GeV^{-1} for us to detect a signal with $\Delta T_s\sim0.5$ K peak value. We have also calculated the probability for the conversion of the photons to axions in the intergalactic magnetic field and find that, for $g_{a\gamma\gamma}\sim10^{-15}$ GeV^{-1},

$$P_{\gamma\to a}=\frac{\epsilon_0c^2}{\hbar^2}g_{a\gamma\gamma}^2B_g^2\frac{Ll}{c^2}\approx10^{-10}\ , \tag{33}$$

where we use for the intergalactic field $B_g=10^{-6}$ G, for the length traversed $L=10$ kpc, and for the Bose oscillation coherence length (for massless axions) $l=3\times10^{19}$ m$=1$ kpc. Thus one would again have to invoke a very large value of $g_{a\gamma\gamma}$ in order to have any substantial flux of axions; these values of $g_{a\gamma\gamma}$ are also excluded by other evidence as discussed in Sec. I.

VII. LIMITS ON AXION PRODUCTION

The apparatus was also used to set limits on the production of axions, or other pseudoscalars, with $m_a/h\leq1$ GHz, as follows: If the cavity is loaded with electromagnetic energy while in the magnetic field, axions will be produced and escape from the cavity volume. Thus the

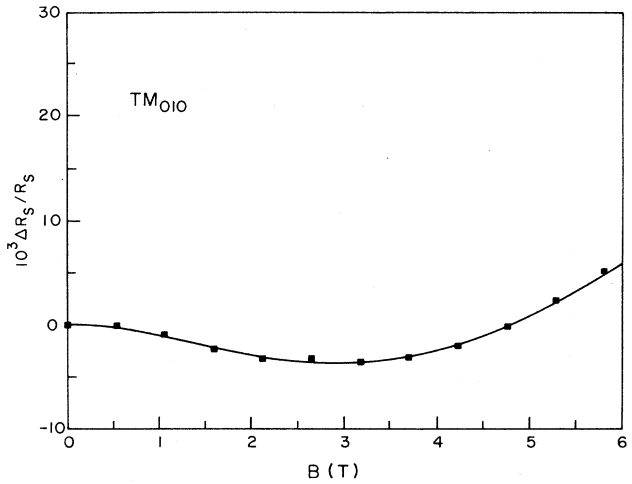

FIG. 20. Fractional change in surface resistance $\Delta R_s/R_s=-\Delta Q/Q$ plotted vs magnetic field for the TM_{010} mode at $f=1.29$ GHz and $T=4.4$ K. For more details see Ref. 43.

magnetic field introduces a new mechanism for energy loss and the cavity Q will be degraded. This effect cannot be separated from Q changes due to the magnetoresistance of the cavity walls, but a limit on its maximum value can be set by measuring $\Delta Q/Q$.

Changes in Q could be measured to a relative accuracy of 10^{-3} and were measured for three different cavity modes.[43] The results for the TM_{010} mode are shown in Fig. 20; here the magnetoresistance is smallest since the current flow is mainly parallel to the field. Contributions from axions can appear only in the TM_{010} mode, and from the data we conclude that the limit on axion production is $\Delta Q/Q<2\times10^{-3}$. From Eq. (21) we calculate the theoretical probability rate for the conversion $\gamma\rightarrow a$ in our apparatus; using $g_{a\gamma\gamma}=10^{-15}$ GeV^{-1}, we find $R_{\gamma\rightarrow a}=10^{-17}$ s^{-1}.

The power in axions P_a is given by

$$P_a=\omega_a\frac{dN_a}{dt}=\omega_a N_\gamma R_{\gamma\rightarrow a}=UR_{\gamma\rightarrow a} \tag{34}$$

with N_γ the number of photons, and U the energy stored in the cavity. Furthermore

$$Q=\frac{U\omega}{P_{\rm loss}}\ ,$$

and from the experimental data

$$\frac{P_a}{P_{\rm loss}}=\frac{U}{P_{\rm loss}}R_{\gamma\rightarrow a}=\frac{Q}{\omega}R_{\gamma\rightarrow a}<2\times10^{-3}\ . \tag{35}$$

Thus, if we use $Q=5\times10^4$ and $\omega=2\pi\times1.25$ GHz, we find from Eq. (35)

$$R_{\gamma\rightarrow a}<\frac{2\times10^{-3}}{Q/\omega}=10^2\ \text{s}^{-1}\ . \tag{36}$$

Comparing this result with the expected rate, and using the quadratic dependence of $R_{\gamma\rightarrow a}$ on $g_{a\gamma\gamma}$, we establish the limit

$$g_{a\gamma\gamma}<10^{-6}\ \text{GeV}^{-1}\ . \tag{37}$$

This result is weaker than the astrophysical limit but has no theoretical uncertainty whatsoever. It pertains only to particles of mass $m_a\leq10^{-6}$ eV, but provides an unambiguous limit on the coupling of light pseudoscalars[44] to two photons.

VIII. CONCLUSIONS

We have set various laboratory limits on the existence of light particles such as axions with masses near 10^{-5} eV that couple to two photons. Upper limits on $g_{a\gamma\gamma}$ at the 95% confidence level for an axion density of 5×10^{-25} g/cm^3 vary from 2.4×10^{-14} GeV^{-1} at $m_a=4.5\times10^{-6}$ eV to 4.2×10^{-13} GeV^{-1} at $m_a=1.6\times10^{-5}$ eV for a narrowly peaked axion line. For a DFS axion with a continuum spectrum, we set the limit $\langle d\rho/df\rangle_a\leq400$ MeV/cm^{3}Hz. A search for a wide axion line near the hydrogen emission frequency of 1.4204 GHz has given negative results. Finally, we establish $g_{a\gamma\gamma}<10^{-6}$ GeV^{-1}, if $m_a\leq10^{-6}$ eV, from the limit on axion production in the cavity. While these limits do not resolve the question of an axion-dominated universe, they are relevant to some recently proposed theoretical models.[45] Second-generation cosmic axion detection experiments with increased sensitivity are presently under active discussion.[46]

ACKNOWLEDGMENTS

It is a pleasure to acknowledge the continuing support of Brookhaven National Laboratory where this work was carried out, and in particular of the AGS division headed by D. Lowenstein. We thank R. Howard, J. Kan, R. Cameron, and M. Swain for assistance in data taking and analysis. We are also indebted to the cryogenics group under H. Hildebrand, the magnet group under G. Ganetis, and the vacuum group under J. Briggs for technical support throughout the experiment. We thank Dr. T. Weiland of DESY for permission to use the program URMEL-T. This work was supported by the U.S. Department of Energy.

*Present address: CERN, 1211, Geneva 23, Switzerland.
†Present address: Sincrotrone Trieste, 34012 Trieste, Italy.

[1]F. Zwicky, Helv. Phys. Acta **6**, 110 (1933).
[2]J. Yang, M. S. Turner, G. Steigman, D. N. Schramm, and K. A. Olive, Astrophys. J. **281**, 413 (1984); for a review of primordial nucleosynthesis, see A. M. Boesgard and G. Steigman, Annu. Rev. Astron. Astrophys. **23**, 319 (1985).
[3]Hot dark matter is a generic term which refers to highly relativistic dark matter. Cold dark matter has very low velocities.
[4]The limit on the electric dipole moment of the neutron is $(\text{EDM})_n\leq10^{-25}$ e cm from D. Dubbers, Nucl. Instrum. Methods A **264**, 120 (1988).

[5]R. Peccei and H. Quinn, Phys. Rev. Lett. **38**, 1440 (1977); Phys. Rev. D **16**, 1791 (1977).
[6]S. Weinberg, Phys. Rev. Lett. **40**, 223 (1978); F. Wilczek, *ibid.* **40**, 279 (1978).
[7]Y. Asano *et al.*, Phys. Lett. **107B**, 159 (1981).
[8]J. Kim, Phys. Rev. Lett. **43**, 103 (1979).
[9]M. Dine, W. Fischler, and M. Srednicki, Phys. Lett. **104B**, 199 (1981).
[10]J. E. Kim, Phys. Rep. **150**, 1 (1987).
[11]G. Raffelt and D. Seckel, Phys. Rev. Lett. **60**, 1793 (1988); M. S. Turner, *ibid.* **60**, 1797 (1988).
[12]J. Preskill, M. B. Wise, and F. Wilczek, Phys. Lett. **120B**, 127 (1983); L. F. Abbott and P. Sikivie, *ibid.* **120B**, 133 (1983); M. Dine and W. Fischler, *ibid.* **120B**, 137 (1983).
[13]M. S. Turner, Phys. Rev. D **33**, 889 (1986).
[14]G. Knapp, S. Tremaine, and J. Gunn, Astrophys. J. **83**, 1585 (1978).
[15]L. Krauss, J. Moody, F. Wilczek, and D. E. Morris, Phys. Rev. Lett. **55**, 1797 (1985).
[16]J. Rogers, Ph.D. dissertation, University of Rochester Report No. UR-1021, 1987.
[17]P. Sikivie, Phys. Rev. Lett. **51**, 1415 (1983); **52**, 695 (1984).
[18]H. Primakoff, Phys. Rev. **81**, 899 (1951).
[19]For a detailed discussion of how the signal and noise depend on coupling, amplifier noise properties, etc., see B. E. Moskowitz and J. Rogers, Nucl. Instrum. Methods A **264**, 445 (1988).
[20]S. De Panfilis *et al.*, Phys. Rev. Lett. **59**, 839 (1987).
[21]Hitachi Ltd. alloy number 101-OFE-HIT, distributed by Copper and Brass Sales, N. Attleboro, MA 02763.
[22]Electroglo, available from Electroglo Co., Chicago, IL 60624. A solution of 25% Electroglo and 75% phosphoric acid was used with a current density of 0.015–0.020 A/cm^2 at the cavity surface for about 15 min.
[23]The sapphire crystals were grown by Saphikon, Inc., Milford, NH 03055. After manufacture, the rods were annealed in a vacuum furnace at 1550 °C for 8 h and then ground to their final diameters.
[24]J. Bamberger, G. Mulholland, A Prodell, H. Worwetz, and C. Whetstone, Adv. Cryog. Eng. **13**, 132 (1967).
[25]The circulators were manufactured by Passive Microwave Technology, Canoga Park, CA. The following models with corresponding frequency ranges were used: LTE 1208 for 1.1–1.4 GHz, LTE 1212K for 1.4–1.9 GHz, STE 1220K for 1.8–2.1 GHz, STE 1221K for 2.1–2.6 GHz, STE 1222K for 2.5–3.5 GHz, CTE 1144K for 3.3–4.6 GHz, and CTE 1145K for 4.3–6.0 GHz. A circulator was not available at the time measurements on cavity 1 were performed.
[26]Micronetics model NSI-11B noise source, available from Micronetics Inc., Norwood, NJ 07648.
[27]S. De Panfilis and J. Rogers, IEEE Trans. Microwave Theory Tech. **36**, 607 (1988).
[28]S. Weinreb, D. Fenstermacher, and R. Harris, National Radio Astronomical Observatory Report No. 220 (unpublished).
[29]The following room-temperature amplifiers, manufactured by Miteq, Inc., Hauppauge, NY, were used: model AM-3A-1020 for the frequency range 1–2 GHz, and model AFD4-020060-30 for the range 2–6 GHz. The noise temperatures were 200 and 300 K with gains of 35 and 40 dB, respectively.
[30]See, e.g., R. B. Blackman and J. W. Tukey, *The Measurement of Power Spectra* (Dover, New York, 1958). The factor of 2π previously published by B. E. Moskowitz, Nucl. Instrum. Methods A **264**, 98 (1988), Eq. (15), is in error.
[31]W. U. Wuensch, Ph.D. dissertation, University of Rochester Report No. UR-1093, 1988.
[32]This "local averaging" is used to remove systematic effects due to changes in amplifier characteristics, etc., which occur over frequency bandwidths much greater than the multiplexer channel width.
[33]$\sigma_{\rm local}$ replaces σ_n to more accurately represent any nonstatistical fluctuations present locally in the data.
[34]Except for cavity 2, for which there was only one reliable pass.
[35]T. Weiland, Nucl. Instrum. Methods **216**, 329 (1983); DESY Report No. 86-106, ISSN 0418-9833 (unpublished).
[36]A listing of the frequency "holes" may be found in BNL E-805 Technical Memo No. 1, 1989 (unpublished), available upon request.
[37]The limit given here for the frequency range 1.090–1.218 GHz from cavity 1 with the 1.486-cm rod differs somewhat from our limit previously given in Ref. 20. This is due to two factors: first, the factor of 2π in Ref. 20, footnote 17 is incorrect; second, the previous result was for the 5σ level of peak-checking without any margin of error for the 95% C.L.
[38]This is a 4% effect as can be seen by comparing the spectra shown in Figs. 15(b) and 16(b).
[39]Partly because of the image rejection circuit.
[40]This is an improvement by a factor of 4 over the results of Ref. 20 where $dP_a/df < 6\times10^{-24}$ W/Hz is reported at $f = 1.090$ GHz.
[41]K. Zioutas and Y. Semertzidis, Phys. Lett. A **130**, 94 (1988) have proposed that HI emitters from distant Infrared Astronomy Satellite galaxies may be point sources of axions. However the photon flux at $f = 1.4$ GHz from these sources is typically 10^{-8} of the galactic flux and therefore the axion flux must be correspondingly suppressed. The relative yield of axions to photons is of order $g_{a\gamma\gamma}m_e$, with m_e the electron mass, so that $a/\gamma \sim 10^{-12}$–10^{18}.
[42]The spectrum without the magnetic field, Fig. 19(c), appears flatter than the corresponding spectra with the field on, Figs. 19(a) and 19(b). This may be due in part to pressure (and thus temperature) fluctuations related with heating of the magnet leads.
[43]J. T. Rogers *et al.*, Appl. Phys. Lett. **52**, 2266 (1988), and references therein.
[44]By using the TE modes one can set limits on the production of scalars as well.
[45]T. Bhattacharya and P. Roy, Phys. Rev. Lett. **59**, 1517 (1987).
[46]*Proceedings of the Workshop on Cosmic Axions,* edited by C. Jones (World Scientific, Singapore, 1989).